Ionic effects on viral DNA packaging and portal motor function in bacteriophage ϕ29

Derek N. Fuller*, John Peter Rickgauer*, Paul J. Jardine†, Shelley Grimes†, Dwight L. Anderson†‡, and Douglas E. Smith*§

*Department of Physics, University of California, San Diego, Mail Code 0379, 9500 Gilman Drive, La Jolla, CA 92093; and Departments of †Diagnostic and Biological Sciences and ‡Microbiology, University of Minnesota, 18-246 Moos Tower, 515 Delaware Street SE, Minneapolis, MN 55455

Edited by Michael Levitt, Stanford University School of Medicine, Stanford, CA, and approved May 14, 2007 (received for review February 14, 2007)

In many viruses, DNA is confined at such high density that its bending rigidity and electrostatic self-repulsion present a strong energy barrier in viral assembly. Therefore, a powerful molecular motor is needed to package the DNA into the viral capsid. Here, we investigate the role of electrostatic repulsion on single DNA packaging dynamics in bacteriophage ϕ29 via optical tweezers measurements. We show that ionic screening strongly affects the packing forces, confirming the importance of electrostatic repulsion. Separately, we find that ions affect the motor function. We separate these effects through constant force measurements and velocity versus load measurements at both low and high capsid filling. Regarding motor function, we find that eliminating free Mg^{2+} blocks initiation of packaging. In contrast, Na^+ is not required, but it increases the motor velocity by up to 50% at low load. Regarding internal resistance, we find that the internal force was lowest when Mg^{2+} was the dominant ion or with the addition of 1 mM Co^{3+}. Forces resisting DNA confinement were up to ≈80% higher with Na^+ as the dominant counterion, and only ≈90% of the genome length could be packaged in this condition. The observed trend of the packing forces is in accord with that predicted by DNA charge-screening theory. However, the forces are up to six times higher than predicted by models that assume coaxial spooling of the DNA and interaction potentials derived from DNA condensation experiments. The forces are also severalfold higher than ejection forces measured with bacteriophage λ.

optical tweezers | single molecule

During the assembly of many dsDNA viruses, the genome is compacted to near-crystalline density (1). Because the size of viral capsids is on the order of the persistence length of the DNA (≈50 nm), significant DNA bending must occur during packaging (2–7). Moreover, due to the negatively charged phosphate backbone of DNA, a large repulsive electrostatic barrier must be overcome during DNA confinement (2–7). In some cases, more than half of the physically available space inside the capsid is taken up by the viral genome (1, 7).

In the case of bacteriophage ϕ29, the 19.3-kbp genome (≈6.5 μm in length) is packed inside a prolate icosahedral capsid ≈45-nm wide and 54-nm long (8). As with many other dsDNA viruses, DNA is translocated into the preformed precursor capsid (prohead) by an ATP-powered molecular motor (9–11). The ϕ29 motor is situated at a unique vertex of the prohead and consists of a ring of RNA molecules (pRNA) sandwiched between two protein rings: the head–tail connector (gene product 10, gp10) and the packaging ATPase (gp16) (12).

Previously, we developed an optical tweezers assay that allowed us to measure the packaging of a single DNA molecule into a single ϕ29 prohead (9). We found that the rate of packaging decreased during capsid filling or when an external force was applied to the DNA substrate. From these measurements, we showed that a large internal force builds during packaging because of DNA confinement and that the motor needs to generate high forces to successfully package its entire genome. We suggested that the internal force that builds during packaging could facilitate the ejection of the DNA that occurs when the virus infects a host cell.

Many investigators have worked on theoretical modeling of viral DNA packaging. Building on earlier work by Riemer and Bloomfield (2) and Odijk (3), Kindt *et al.* (4), Tzlil *et al.* (5), and Purohit *et al.* (6, 7) used analytical theory to predict the forces involved in packaging. In a coarse-grained Brownian dynamics simulation using a harmonic bending potential and Lennard–Jones (attractive–repulsive) interaction potential, Kindt *et al.* observed spontaneous arrangement of the DNA into a toroidal structure, which expanded into a spool-like structure toward the latter stages of packaging. Kindt *et al.* and Tzlil *et al.* performed complementary analytical calculations that assumed local hexagonal order and uniaxial symmetry and allowed for arbitrary cross-sectional shapes of the packed DNA, as determined by energy-functional minimization (4, 5). They predicted forces resisting packaging on the order of tens of piconewtons for bacteriophage λ. Purohit *et al.* made similar calculations for the case of several different viruses (capsid geometries) in which the DNA strands were assumed to be packed in a hexagonal lattice that forms an inverse spool coaxial to the portal channel (6, 7). Cryo-EM reconstructions of some phages suggest that the DNA is at least partially organized in a coaxial spool (13–17), although the degree of order toward the interior (away from the capsid wall) remains unclear. X-ray diffraction studies of phages have consistently revealed short-range interaxial DNA separations of 2–3 nm (1). Several recent theoretical models (4–7) have used empirical DNA–DNA interaction potentials deduced from x-ray diffraction measurements on DNA condensed in solution by polyethylene glycol (18, 19) or by fitting the model to our previous optical tweezers data (7).

The inverse spool model is very useful for comparison with experimental data as the parameters may be fixed according to independently measured quantities, and the internal force may be quickly calculated for a given set of parameters. A significant dependence of the packaging forces on ionic conditions and on the type of phage (i.e., capsid volume, shape, and genome length) is predicted (7). For example, in equivalent ionic conditions, bacteriophage λ is predicted to have a substantially greater internal force than ϕ29 (6). However, recent studies of bacteriophage λ find that DNA ejection can be inhibited by applying osmotic pressure (20), permitting an estimate of the maximum internal force of ≈20 pN (21, 22). Rather than being higher, this force is at least 3-fold lower than the maximum internal force in ϕ29 (9). However, the ionic conditions used in these studies were different. It is possible that the lower forces measured with λ

Author contributions: D.N.F., J.P.R., P.J.J., S.G., D.L.A., and D.E.S. designed research; D.N.F., J.P.R., P.J.J., S.G., and D.E.S. performed research; D.N.F., J.P.R., and D.E.S. analyzed data; and D.N.F., J.P.R., P.J.J., S.G., D.L.A., and D.E.S. wrote the paper.

The authors declare no conflict of interest.

This article is a PNAS Direct Submission.

See Commentary on page 11125.

§To whom correspondence should be addressed. E-mail: des@physics.ucsd.edu.

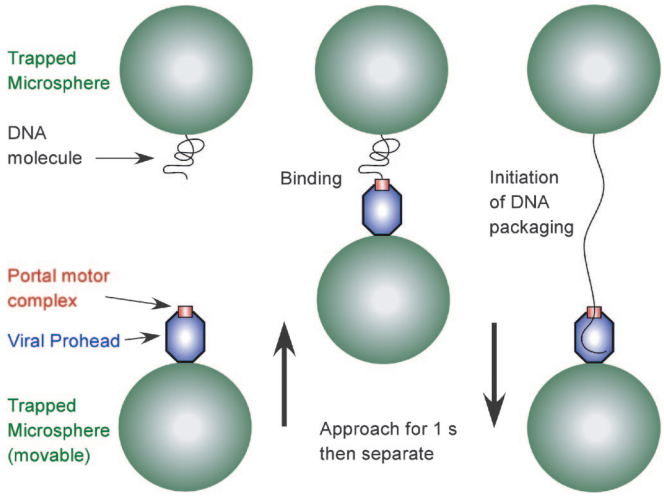

Fig. 1. Schematic illustration of the experiment. (*Bottom Left*) Prohead–motor complexes were attached to antibody-coated microspheres and captured in one optical trap. (*Top Left*) Biotinylated DNA molecules were tethered to streptavidin-coated microspheres and captured in a second optical trap. The bottom trap was moved with respect to the top one while measuring the DNA tension. To initiate packaging, the microspheres were brought into near contact for ≈1 s (*Middle*) and then quickly separated to probe for DNA binding and translocation (*Right*).

could be due to the ionic screening being higher in those experiments.

It is well known that cations bind to DNA in solution and lower its effective charge density (23). DNA condensation studies indicate that the interstrand repulsion varies significantly with a change in valence of the cation screening the DNA (18, 19). Therefore, we expect that if we change the ionic environment, we will modulate the internal electrostatic forces. If electrostatic repulsion is indeed the largest contributing factor to the internal force, as predicted theoretically (2), a small change in this screening should have a significant effect on the forces resisting DNA compaction. Here, we investigate such effects through measurements of single DNA packaging dynamics with optical tweezers.

Results and Discussion

Optical Tweezers Measurements. The packaging of single DNA molecules into single ϕ29 proheads was measured using a new approach that allows the entire process to be measured from initiation to completion with improved accuracy. This approach was essential for quantifying differences in varying ionic conditions. DNA packaging was initiated dynamically during the optical tweezers measurement by using a DNA substrate lacking the ϕ29 terminal protein, gp3. We recently found that gp3 causes variability in the measured DNA lengths in the optical tweezers, most likely due to gp3-induced DNA looping, which interferes with accurate determination of the amount of DNA packaged (J.P.R., D.N.F., S.G., P.J.J., D.L.A., and D.E.S., unpublished manuscript). Here we also use a dual optical tweezers system that provides more accurate tether-length determination compared with the single-trap/pipette system used in ref. 24. Preassembled prohead-gp16 motor complexes were attached to antibody-coated microspheres, and biotin-tagged DNA molecules were tethered to streptavidin-coated microspheres. Each type of microsphere was captured in a separate optical trap, and packaging was initiated by bringing them into near contact in the presence of ATP (Fig. 1).

Two measurement modes were used. In the first method, a constant load ("force-clamp") was applied to keep tension on the DNA tether by using a feedback system to control the separation between the two traps, permitting DNA translocation to be tracked continuously throughout the process of packaging. These measurements yield data on the rate of packaging (motor velocity) versus length of DNA packaged (capsid filling). A force clamp of 5 pN was used because it kept the DNA extended to facilitate accurate measurement of the DNA length while minimally perturbing the motor (9, 10). In the second method, the trap positions were fixed and the motor worked against a steadily building DNA tension, yielding data on the velocity versus load relationship. Data from these two types of measurements were then compared to infer the internal force resisting DNA confinement as a function of capsid filling.

Conditions That Support Initiation and Packaging. Divalent cations have a greater potential for screening than monovalent cations, and when multiple ions are present, ion species compete to screen the DNA (25). We sought to explore the widest range of screening conditions in which we could measure packaging (Table 1). We started with the standard packaging buffer used in many previous *in vitro* studies: 25 mM Tris·HCl (pH 7.8), 50 mM NaCl, and 5 mM $MgCl_2$ (12). In this buffer, both the Na^+ and Mg^{2+} ions contribute to screening. To achieve lower screening (higher net DNA charge), we attempted to reduce Mg^{2+} to zero but found that a minimum of ≈1 mM free Mg^{2+} (aside from that complexed with ATP) was needed for packaging initiation. Therefore, to achieve our lowest screening (highest net charge) we used 1 mM Mg^{2+} plus 100 mM Na^+, such that Na^+ would be the dominant counterion (Table 1). To achieve higher screening (lower net DNA charge), Na^+ was eliminated, and Mg^{2+} was increased up to 30 mM to ensure that it would be the dominant ion screening the DNA (Table 1). In addition, the effect of adding 1 mM Co^{3+} (from cobalt hexamine), a stronger screening agent, to the standard packaging buffer was studied. Higher

Table 1. Ionic conditions studied and motor velocity

Condition	Na^+, mM	Mg^{2+}, mM	Co^{3+}, mM	Percent screening of DNA charge	Average velocity, bp/s
High Na^+	100	1	0	80.4	170 ± 4
Standard	50	5	0	84.9	145 ± 5
High Na^+ and Mg^{2+}	50	50	0	88.2	149 ± 4
Moderate Mg^{2+}	0	5	0	88.2	114 ± 5
High Mg^{2+}	0	30	0	88.6	141 ± 4
Standard + Co^{3+}	50	5	1	90.7	165 ± 4

The percent screening of DNA charge was calculated according to the modified Manning two-species counterion competition theory (23, 25). The monovalent ions were neglected in the Co^{3+} calculation, such that the figure is an upper bound. Each solution also contained 25 mM Tris·HCl (pH 7.6), except for the moderate and high Mg^{2+} solutions, in which Tris·HCl was lowered to 1 mM so as to minimize potential competition between $Tris^+$ and Mg^{2+}. The average velocity is in the limit of zero capsid filling with 5 pN of applied load.

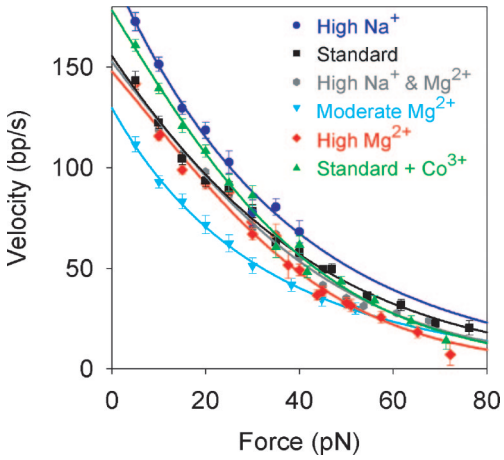

Fig. 2. Dependence of the average motor velocity on force was determined from measurements on $n = 25–58$ complexes (mean $n = 38$) for selected ionic conditions. Error bars report standard errors. The different colors and symbols indicate the different ionic conditions studied, as described in Table 1. The lines are fits of the data to a theoretical model (10), as explained in *Methods*.

concentrations of Co^{3+} were not used because these induce DNA condensation (26), which interferes with our method of initiating packaging.

Effect of Ions on Motor Function. We characterized the dependence of the motor velocity on load by using the fixed-trap separation mode (Fig. 2). Measurements up to ≈40 pN were made at low-capsid filling, at which internal force contributes little to the total force. At >40 pN, DNA tether failure occurs frequently. To access higher forces, we made additional measurements with complexes at ≈70–80% filling, at which internal force contributes substantially to the net force on the motor. The overall trend of decreasing velocity with increasing load was similar in each ionic condition, but differences in the magnitudes of the velocities and shapes of the curves were observed. We find that as Na^+ increases, the initial motor velocity increases. At low load and low capsid filling, the highest speed (170 bp/s) was measured in the buffer containing 100 mM Na^+, whereas the lowest speed (114 bp/s) was observed with 0 mM Na^+ and 5 mM Mg^{2+}.

Our finding that free Mg^{2+} (aside from that bound in Mg^{2+}-ATP) is required for initiation of packaging, suggests that Mg^{2+} is a cofactor for motor function, as is the case with many DNA directed enzymes including polymerases, helicases, and endonucleases (27). In contrast, Na^+ is not required, but its presence increases the motor velocity. Some models for motor function have proposed that electrostatic interactions between charged residues in the motor and the negatively charged DNA may be responsible for DNA translocation (28). However, our data are not completely consistent with this idea. Although higher motor velocity was observed with Na^+ screening (highest DNA charge) than with Mg^{2+} screening (lower DNA charge), higher velocity was also recorded with added Co^{3+} (lower DNA charge than with Na^+). These results suggest that there is a direct effect of cations on the structure (29) and performance of the motor complex, rather than just a modulation of the DNA–motor electrostatic interactions.

Dependence of the Packaging Rate on Capsid Filling. Velocity versus filling plots obtained in different ionic conditions are shown in Fig. 3*A*. In each condition, the velocity decreases monotonically with filling. However, the magnitudes of the initial velocities varied, and there were qualitative differences in the shape of the curves. In particular, in the three higher screening conditions, a plateau was observed in which the velocity decreased minimally for fillings up to ≈30%. In contrast, in the three conditions with lower screening, no such plateau was observed. In all cases, a sharp drop in the velocity was observed above ≈50% filling, and in all but one condition, the velocity converged toward zero at ≈100% genome length packaged. The exception was in the high Na^+ buffer (with highest net DNA charge), in which the velocity approached zero at ≈90% filling, indicating that packaging would not proceed to completion under this condition. The velocity in the standard packaging buffer at low filling is higher than reported earlier (9). This finding is attributable to the fact that velocity decreases with filling and, as discussed above, we measure at lower filling and with improved accuracy in the present work.

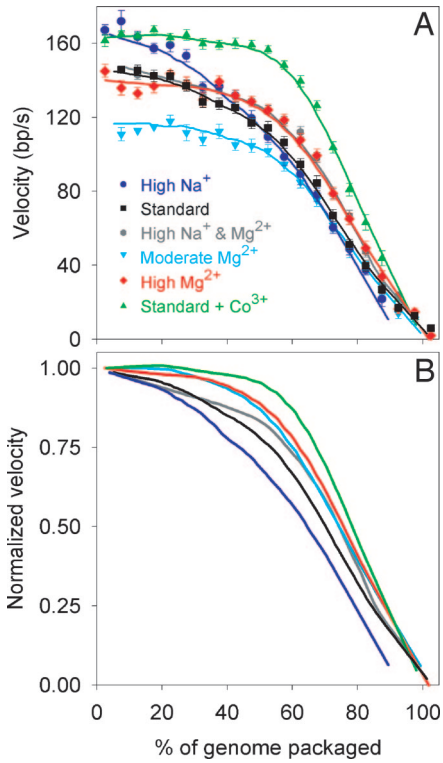

Fig. 3. Velocity decrease due to filling. (*A*) Dependence of the average rate of packaging on capsid filling (expressed as percent of the native ϕ29 genome packaged) for selected ionic conditions. The measurements were made using the force-clamp method with $F = 5$ pN. The different colors and symbols indicate the different ionic conditions studied, which are described in Table 1. Points are averages in bins over $n = 26–59$ individual data sets (mean $n = 36$). The solid lines were obtained by filtering of the raw velocity data for all complexes (see *Methods*). (*B*) Velocity normalized by the maximum velocity. For clarity, only the smoothed lines from *A* are plotted.

There is no simple trend of increasing absolute packaging rate with increasing ionic screening, as would be expected if screening of internal DNA packing forces were the only factor governing the packaging rate. This lack of a simple trend is due to the fact that ions affect the motor function, as discussed in the previous section. When the velocities are normalized by their maximum values at low filling, the plots are distributed in accord with the expected trend of ionic screening over most of the range of capsid fillings (Fig. 3*B* and Table 1).

Internal Forces Resisting DNA Confinement. We deduce the dependence of the internal force on capsid filling by correlating velocity versus force and velocity versus filling data sets measured under identical ionic conditions (Figs. 2 and 3), as shown

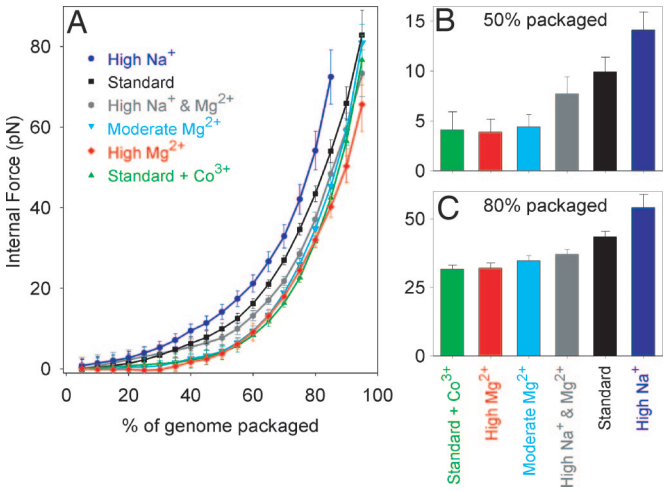

Fig. 4. Force resisting DNA packaging. (*A*) Internal force versus capsid filling for selected ionic conditions. The different colors and symbols indicate the different ionic conditions studied. (*B* and *C*) Internal forces with either 50% (*B*) or 80% (*C*) of the genome packaged versus ionic condition. The colors matched those used in *A*. The *y* axis in *B* and *C* share the same units as the plots in *A*, and *B* has the same *x* axis label as *C*.

in Fig. 4. This analysis allows us to isolate the effect of ions on packing forces from their effect on motor function. Qualitatively, the magnitude of the internal force across the entire range of fillings follows the expected trend with ionic screening (Table 1). The highest forces were measured with Na^+ as the dominant counterion, and considerably lower forces were measured with Mg^{2+} dominant. Similar trends have recently been found in studies of DNA ejection from bacteriophage λ. Bulk experiments using osmotic pressure to inhibit ejection find shorter lengths of DNA ejected with Mg^{2+} as the dominant ion compared with Na^+, implying lower internal pressure (A. Evilevitch, C. Knobler, and W. Gelbart, personal communication), and fluorescence imaging experiments find slower ejection rates with Mg^{2+} than with Na^+ (P. Grayson, L. Han, T. Winther, and R. Phillips, personal communication).

In our experiments, reduced internal forces similar to those with high Mg^{2+} were also observed with 1 mM Co^{3+} added to the standard buffer, thus illustrating that trivalent cations can screen the DNA very effectively, even when in competition with higher concentration mono- and divalent cations. We also observed qualitative differences in the shape of the force versus filling curves dependent on ionic conditions. In particular, a plateau of near-zero internal force is observed during the first one-third of packaging with the high Mg^{2+} and Co^{3+} buffers, but not with the lower-screening buffers. Such a plateau is in qualitative accord with the predictions of the coaxial spool model (7). In all conditions, the internal force rose sharply with capsid filling to >60 pN. In the high Na^+ and standard buffers, the force clearly extrapolates to >100 pN with the full ϕ29 genome length of DNA packaged.

Comparisons with Theory. DNA packaging forces have been calculated theoretically for the specific case of bacteriophage ϕ29, and we can directly compare our findings with these predictions (6, 7). This model assumes that the DNA is spooled in a hexagonal array circling about the long axis of the capsid. The capsid was modeled as a cylinder capped by two hemispheres, and the capsid volume was estimated from cryo-EM 3D reconstructions (7, 8). The free energy required to package the DNA was calculated considering an elastic bending term, treating the DNA as a worm-like chain with a 50-nm persistence length and a DNA–DNA interaction potential. The assumed form of the interaction potential G_{int} was derived empirically from experiments in which DNA segments were condensed into hexagonally packed bundles in solution by applied osmotic pressure, accounting for electrostatic interactions, ionic screening, entropic effects, and hydration effects (4, 7, 18, 19). Specifically, $G_{\rm int} = \sqrt{3}F_0(c^2 + cd_s)L\ \exp(-d_s/c)$, where d_s is the interaxial spacing between the DNA strands, L is the total DNA length, and c and F_0 are constants determined from the condensation experiments (dependent on ionic conditions) (18, 19). The total free energy was then minimized by varying d_s given a certain DNA length confined in the capsid, and the internal resisting force was calculated as the derivative of the energy with respect to the length of DNA packaged (7). This model thus makes the additional simplifying assumption that the DNA conformation equilibrates to the minimum energy state at all time points during packaging and that there is no energy dissipation due to friction.

The results of these calculations are in qualitative agreement with our experimental findings in that the internal force rises sharply at the final stages of filling, and the magnitude increases with decreasing ionic screening. However, the agreement between experiment and this theory is not quantitative. In our high Na^+ buffer, in which Na^+ is the dominant ion screening the DNA, we find an internal force of ≈72 pN at 85% filling, extrapolating to >100 pN at 100% filling. By comparison, using values of $c = 0.35$ nm and $F_0 = 1.7 \times 10^4$ pN/nm^2 appropriate for the case of 50 mM Na^+, the model predicts internal force of ≈50 pN at 100% filling. This value is also lower than the ≈65 pN we find at 90% filling with 50 mM Na^+ and 5 mM Mg^{2+}, a higher screening condition than 50 mM Na^+ alone. An even greater difference is found when Mg^{2+} is the dominant screening counterion. Using $c = 0.30$ nm and $F_0 = 1.2 \times 10^4$ pN/nm^2 appropriate for 25 mM Mg^{2+}, the model predicts internal forces of ≈2, ≈5, and ≈10 pN at capsid fillings of 50%, 75%, and 95%, respectively (P. K. Purohit, personal communication), whereas we find ≈4, ≈25, and ≈65 pN, respectively, in our high Mg^{2+} buffer.

Several factors may potentially contribute to the discrepancy between the experiments and theory. First, the DNA in ϕ29 may not be packaged as a coaxial spool, as the theoretical model assumes, and the conformation may also be different from that in phage λ. The model predicts different internal forces for different bacteriophages, dependent on capsid size, shape, and genome length (7). A maximum internal force of ≈20 pN in 10 mM $MgCl_2$ has been reported for phage λ on the basis of experiments in which osmotic pressure was used to inhibit DNA ejection (21), and this finding is in good agreement with the model predictions (7). However, in equivalent ionic conditions (50 mM Na^+, 5 mM Mg^{2+}), the model predicts a 40% higher maximum internal force with phage λ than with ϕ29 (7), whereas we find higher internal forces with ϕ29. Specifically, in our high Mg^+ buffer, we find ≈65 pN at 95% filling, extrapolating to >80 pN at 100% filling. Because this measurement was done with an equivalent or higher screening condition (30 mM Mg^{2+}) than that used in the phage λ DNA ejection measurements (10 mM Mg^{2+}), the difference is not attributable to differences in electrostatic screening.

Recent cryo-electron microscopy 3D reconstructions of P22 and epsilon15 virions (15–17) indicate at least partial spooling of the DNA around the portal axis; however, similar reconstructions of ϕ29 do not appear to indicate such coaxial organization, especially in the early stages of packaging (L. Comolli, A. Spakowitz, C. Siegerist, S.G., P.J.J., D.L.A., C. Bustamante, and K. Downing, unpublished manuscript). In addition, several molecular dynamic simulations of packaging do not observe spontaneous DNA spooling (4, 30–34). A tendency for coaxial spooling was primarily observed in simulations which assumed an attractive DNA–DNA

potential, as would only be found with DNA condensing polyamines present (4), and in simulations that assumed an internal protein spindle inside the capsid, as occurs in phage T7 (33). According to several recent dynamic simulations, differences in DNA organization may occur because of differences in shape (32), rate of DNA packaging (33), and level of DNA twisting (31). Besides DNA conformation, another potential cause for discrepancies is uncertainty in the estimated capsid volumes, which could have a significant effect on the calculated force, particularly at high filling (7). An ≈5% overestimate in the determination of the linear dimensions of the capsid by cryo-electron microscopy would lead to as much as a factor of two underestimate in the calculated internal force in the Mg^{2+} screening case (7, 22) (P. Grayson, personal communication).

Second, energy dissipation may occur during packaging, such that the measured work done is higher than the gain in potential energy. This effect may explain our finding of a higher internal force than predicted and found for DNA ejection in λ (7, 21). Gabashvili and Grosberg (35) and Odijk (36) have suggested that there may be significant friction between DNA segments inside the capsid when such segments are moving during packaging and ejection. However, quantitative predictions for such friction have not been presented. Observations of occasional, rapid slipping during ϕ29 DNA packaging (9) and of DNA ejection from bacteriophages T5 (37) and λ (P. Grayson, L. Han, T. Winther, and R. Phillips, personal communication) at rates at least two orders of magnitude faster than the rate of packaging suggest that the friction may be negligible.

Finally, another possible reason for the discrepancy could be that the DNA–DNA interaction potentials used in theoretical calculations may not be universally applicable in describing the DNA packaged in all types of phages in all ionic environments. The potentials used were derived empirically from experiments in which straight DNA segments were condensed into hexagonally packed bundles in solution by applied osmotic pressure (18, 19). Although the theoretical models of phage DNA packaging referred to above explicitly include bending energy, it is possible that bent DNA segments would not obey exactly the same interaction potentials as straight ones (although this may be a small correction if the bending occurs on a scale much larger than the interaction distance). In addition, the dynamic conformation adopted by the DNA during rapid packaging may not be exactly equal to the equilibrated free-energy minimum conformation. Recent studies of DNA knotting in phage P4 suggest that the DNA can rearrange after packaging (38), and recent molecular dynamics simulations confirm this notion and indicate that ejection forces are lower than packaging forces if the DNA is given time to relax before it is ejected (32). Such effects may contribute to our finding of a higher internal force than predicted theoretically and a higher internal force during packaging with phage ϕ29 than that found driving ejection in phage λ.

Conclusions

We report significant effects of ionic screening on DNA packaging in ϕ29, thus quantifying the importance of electrostatic repulsion during this process. Ions were shown to affect both the physics of DNA confinement and the function of the packaging motor. These effects were dissected by means of velocity versus filling and velocity versus force measurements in various ionic conditions. We show that ionic effects cannot account for the higher internal forces measured with phage ϕ29 than measured during ejection with phage λ. Internal forces opposing DNA confinement in ϕ29 were found to build sharply with increasing filling and decrease in accord with the expected trend of increasing ionic screening. However, the magnitudes of these forces are substantially higher than predicted by current theories.

Materials and Methods

Sample Preparation. Bacteriophage ϕ29 components, including proheads and gp16, were purified as described in ref. 39. A 25,340-bp dsDNA construct labeled at one end with biotin was prepared as described in ref. 24. Because the presence of the ϕ29 DNA terminal protein (gp3) causes large inaccuracy in measuring the packaged DNA length (J.P.R., D.N.F., S.G., P.J.J., D.L.A., and D.E.S., unpublished manuscript), we used a non-gp3 DNA construct in the present work to ensure accurate measurement of capsid filling. Two micrograms of proheads were mixed with 0.25 μg of gp16 in 10 μl of 25 mM Tris·HCl buffer (pH 7.8)/50 mM NaCl/5 mM $MgCl_2$ and incubated for 2 min. γS-ATP (Roche Applied Science, Indianapolis, IN) was then added to a final concentration of 0.4 mM, and the sample was incubated for 45 min at room temperature.

Streptavidin-coated microspheres (2.1-μm diameter, 0.5% wt/vol; Spherotech, Libertyville, IL) and protein G-coated microspheres (2.1 μm diameter, 0.5% wt/vol; Spherotech) were washed in PBS. DNA was tethered to the streptavidin microspheres, and anti-phage antibodies were attached to the protein G microspheres as described in refs. 9 and 24. Two micoliters of microspheres were added to 4.5 μl of the prohead complexes and incubated for 45 min. Packaging measurements were carried out in the buffers listed in Table 1 supplemented with 0.5 mM ATP. Experiments showed that use of a higher concentration of ATP did not increase the rate of packaging, thus indicating that we are operating in the limit of saturating ATP (10).

Optical Tweezers Measurements. The dual-trap apparatus consists of a diode-pumped solid-state Nd:YAG laser (CrystaLaser, Reno, NV) split into two orthogonally polarized beams and focused by a water-immersion microscope objective (Plan Apochromat, 1.2 NA; Olympus, Melville, NY). One beam was steered by use of an acousto-optic deflector (Intraaction, Bellwood, IL). The exiting beams were collected by an identical objective, and the deflections of the fixed beam were measured by imaging the back focal plane of the objective onto a position-sensing detector (On-Trak, Lake Forest, CA). Measurements were done at ≈23°C. The instrument was calibrated by stretching DNA molecules, as described in ref. 40. Force-clamp measurements were made with a feedback loop running at 50 Hz to control the trap position.

Data Analysis. The tether length was computed from the measured extension and force versus fractional extension relationship measured separately in each experimental condition. Force-velocity measurements at $F < 45$ pN were made in the fixed trap position mode at low capsid filling (≈20–30%) and those at $F > 45$ pN at high capsid filling (≈70–80%) where internal force contributed significantly to the total force. The contribution of internal force was determined using the measured velocity-filling relationship and low-force portion of the measured force-velocity relationship. The force-velocity data sets were also corrected to account for the internal force and small change in amount of packaged DNA (from ≈20% to 30%) during the measurement. This correction was small (<5%) and did not affect the overall trend of the internal force with ionic screening. Velocities were calculated by linear fitting in a 1-s sliding window and averaged over all complexes in 5-pN force bins or 5% filling bins. The smoothed lines in Fig. 3 were obtained by negative-exponential filtering the raw (unbinned) velocity measurements for all complexes in 100 intervals with a 5% sampling proportion (Sigmaplot 6.0; SPSS, Chicago, IL). Large pauses ($V < 10$ bp/s for >2 s) that would significantly skew the velocity measured with a given complex at a particular force or filling point were removed before

calculating the mean. The formula used to fit the velocity versus force data in Fig. 2 is $v = 1/(a + b \cdot \exp(c \cdot F))$, where a, b, and c are fit parameters, as shown to be suitable in ref. 10. We used this fit as an interpolation formula to calculate the force corresponding to each velocity measured in the velocity-filling data, to calculate internal force. Errors were estimated using 95% confidence intervals in the fit by using the curve-fitting toolbox in Matlab (Mathworks, Natick, MA).

We thank Victor Bloomfield, Carlos Bustamante, Alex Evilevitch, Bill Gelbart, Paul Grayson, Rachel Millin, Rob Phillips, Prashant Purohit, Dorian Raymer, Ioulia Rouzina, and Al Schweitzer for advice and assistance. Our research was supported by National Institutes of Health Grants GM-071552 and DE-03606, The Burroughs–Wellcome Fund, The Kinship Foundation, and the Arnold and Mabel Beckman Foundation. D.N.F. was also supported by National Institutes of Health Grant P01 DK54441 through the Molecular Biophysics Training Program at the University of California, San Diego.

1. Earnshaw WC, Casjens SR (1980) *Cell* 21:319–331.
2. Riemer SC, Bloomfield VA (1978) *Biopolymers* 17:785–794.
3. Odijk T (1998) *Biophys J* 75:1223–1227.
4. Kindt J, Tzlil S, Ben-Shaul A, Gelbart WM (2001) *Proc Natl Acad Sci USA* 98:13671–13674.
5. Tzlil S, Kindt JT, Gelbart WM, Ben-Shaul A (2003) *Biophys J* 84:1616–1627.
6. Purohit PK, Kondev J, Phillips R (2003) *Proc Natl Acad Sci USA* 100:3173–3178.
7. Purohit PK, Inamdar MM, Grayson PD, Squires TM, Kondev J, Phillips R (2005) *Biophys J* 88:851–866.
8. Tao Y, Olson NH, Xu W, Anderson DL, Rossmann MG, Baker TS (1998) *Cell* 95:431–437.
9. Smith DE, Tans SJ, Smith SB, Grimes S, Anderson DL, Bustamante C (2001) *Nature* 413:748–752.
10. Chemla YR, Aathavan K, Michaelis J, Grimes S, Jardine PJ, Anderson DL, Bustamante C (2005) *Cell* 122:683–692.
11. Jardine PJ, Anderson D (2006) in *The Bacteriophages*, ed Calendar R (Oxford Univ Press, New York), pp 49–65.
12. Grimes S, Jardine PJ, Anderson D (2002) *Adv Virus Res* 58:255–294.
13. Cerritelli ME, Cheng N, Rosenberg AH, McPherson CE, Booy FP, Steven AC (1997) *Cell* 91:271–280.
14. Olson NH, Gingery M, Eiserling FA, Baker TS (2001) *Virology* 279:385–391.
15. Jiang W, Chang J, Jakana J, Weigele P, King J, Chiu W (2006) *Nature* 439:612–616.
16. Lander GC, Tang L, Casjens SR, Gilcrease EB, Prevelige P, Poliakov A, Potter CS, Carragher B, Johnson JE (2006) *Science* 312:1791–1795.
17. Chang J, Weigele P, King J, Chiu W, Jiang W (2006) *Structure (London)* 14:1073–1082.
18. Rau DC, Lee B, Parsegian VA (1984) *Proc Natl Acad Sci USA* 81:2621–2625.
19. Rau DC, Parsegian VA (1992) *Biophys J* 61:246–259.
20. Evilevitch A, Lavelle L, Knobler CM, Raspaud E, Gelbart WM (2003) *Proc Natl Acad Sci USA* 100:9292–9295.
21. Evilevitch A, Castelnovo M, Knobler CM, Gelbart WM (2004) *J Phys Chem B* 108:6838–6843.
22. Grayson P, Evilevitch A, Inamdar MM, Purohit PK, Gelbart WM, Knobler CM, Phillips R (2006) *Virology* 348:430–436.
23. Manning GS (1978) *Q Rev Biophys* 11:179–246.
24. Fuller DN, Gemmen GJ, Rickgauer JP, Dupont A, Millin R, Recouvreux P, Smith DE (2006) *Nucleic Acids Res* 34:e15.
25. Wilson RW, Bloomfield VA (1979) *Biochemistry* 18:2192–2196.
26. Widom J, Baldwin RL (1980) *J Mol Biol* 144:431–453.
27. Cowan JA (1995) *The Biological Chemistry of Magnesium* (Wiley, New York).
28. Doering C, Ermentrout B, Oster G (1995) *Biophys J* 69:2256–2267.
29. Harding MM (2002) *Acta Crystallogr* 58:872–874.
30. Ali I, Marenduzzo D, Yeomans JM (2004) *J Chem Phys* 121:8635–8641.
31. Spakowitz AJ, Wang ZG (2005) *Biophys J* 88:3912–3923.
32. Ali I, Marenduzzo D, Yeomans JM (2006) *Phys Rev Lett* 96: 208102–1-4.
33. Forrey C, Muthukumar M (2006) *Biophys J* 91:25–41.
34. Petrov AS, Harvey SC (2007) *Structure (London)* 15:21–27.
35. Gabashvili IS, Grosberg A (1992) *J Biomol Struc Dyn* 9:911–920.
36. Odijk T (2004) *Philos Transact A Math Phys Eng Sci* 362:1497–1517.
37. Mangenot S, Hochrein M, Radler J, Letellier L (2005) *Curr Biol* 15:430–435.
38. Arsuaga J, Vazquez M, McGuirk P, Trigueros S, Sumners D, Roca J (2005) *Proc Natl Acad Sci USA* 102:9165–9169.
39. Grimes S, Anderson D (1997) *J Mol Biol* 266:901–914.
40. Rickgauer JP, Fuller DN, Smith DE (2006) *Biophys J* 91:4253–4257.